Zincostottite, $ZnGe(OH)_6$, the zinc analogue of stottite from Tsumeb, Namibia

Anthony R. Kampf[1*], Joy Désor[2], Mark D. Welch[3], Chi Ma[4] and Gerhard Möhn[5]

[1] Mineral Sciences Department, Natural History Museum of Los Angeles County, 900 Exposition Boulevard, Los Angeles, CA 90007, USA

[2] Independent researcher, Bad Homburg, Germany

[3] Natural History Museum, London, SW7 5BD, UK.

[4] Division of Geological and Planetary Sciences, California Institute of Technology, Pasadena, California 91125, USA

[5] Independent researcher, Niedernhausen, Germany

*E-mail: akampf@nhm.org

Abstract

The new mineral zincostottite (IMA2024-024), $ZnGe(OH)_6$, was found on specimens from the Tsumeb mine, Tsumeb, Namibia, where it is a secondary oxidation-zone mineral. It occurs as heavily etched remnants of equant or tabular crystals, up to about 1 mm in diameter. Crystals are colourless and transparent, with vitreous to subadamantine lustre and white streak. The mineral is brittle with irregular stepped fracture. The Mohs hardness is about 4.5.

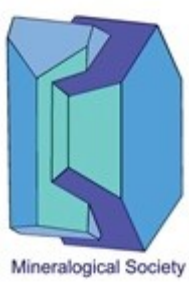

This is a 'preproof' accepted article for Mineralogical Magazine. This version may be subject to change during the production process.
DOI: 10.1180/mgm.2024.81

Cleavage is good on {100} and poor on {001}. The calculated density is 3.834 g·cm^{-3}. Optically, zincostottite is uniaxial (–) with ω = 1.785(5) and ε = 1.765(5) (white light). The empirical formula is $(Zn_{0.77}Fe^{3+}_{0.23})_{\Sigma 1.00}Ge_{1.00}O_6H_{5.77}$. Zincostottite is tetragonal, space group $P4_2/n$, with cell parameters: a = 7.4522(18), c = 7.4000(8) Å, V = 411.0(2) Å^3 and Z = 4. The crystal structure (R_1 = 2.65% for 452 $I > 2\sigma_I$ reflections) is the same as that of stottite with Zn in place of Fe^{2+}.

Keywords: zincostottite; new mineral; stottite; crystal structure; Raman spectroscopy; Tsumeb mine, Tsumeb, Namibia

Introduction

Hydroxyperovskites are frameworks of corner-linked octahedra in which all oxygen atoms form hydroxyl groups and each is a donor and acceptor. The cavity *A*-site of normal perovskites is empty in hydroxyperovskites. Coupled with moderately strong hydrogen bonding, the absence of an *A* cation results in a framework of highly tilted octahedra. Two stoichiometries have been recognized so far, corresponding to single and double hydroxyperovskites, denoted $B(OH)_3$ and $BB'(OH)_6$, respectively, where *B* and *B′* are metal cations. Double hydroxides are combinations of divalent and tetravalent cations, and are predominantly stannates, although a germanate and a silicate (synthetic) are also known. The single exception to the B^{2+}/B'^{4+} combination is mopungite $NaSb(OH)_6$. The crystal chemistry of hydroxyperovskites is reviewed by Mitchell *et al.* (2017). Herein, we describe zincostottite, the second natural germanate hydroxyperovskite. Including the recently approved nancyrossite, there are now 15 natural hydroxyperovskites (Table 1).

Zincostottite is named as the Zn analogue of stottite, $Fe^{2+}Ge(OH)_6$. The new mineral and the name have been approved by the International Mineralogical Association (IMA2024-

https://doi.org/10.1180/mgm.2024.81 Published online by Cambridge University Press

024; Warr symbol: Zsto). The description is based upon one holotype specimen and one cotype specimen deposited in the collections of the Natural History Museum of Los Angeles County, 900 Exposition Boulevard, Los Angeles, CA 90007, USA, catalogue numbers 76278 and 76279, respectively.

Occurrence

Zincostottite was found on specimens from the Tsumeb mine, Tsumeb, Namibia (19°15'S, 17°42'E). An overview of the mineralogy and geology of the Tsumeb deposit can be found in Gebhard (1999) and von Bezing (2007). Zincostottite occurs on fracture surfaces in ore containing a mixture of germanite, chalcocite, bornite and tennantite-(Zn). Other minerals found in association with zincostottite are siderite, malachite and quartz. The specimens come from the collection of Karl Seifert, who was mining engineer at Tsumeb from 1963 to 1967. The 2nd oxidation zone of the deposit was being mined during that period. Zincostottite probably originates from the Ge-rich horizon at Level 30 of the mine, about 900 m below the surface and near the top of the 2nd oxidation zone. Zincostottite is a secondary oxidation-zone mineral.

Physical and optical properties

Zincostottite occurs as heavily etched remnants of equant or tabular crystals, up to about 1 mm in diameter (Fig. 1). No crystal forms could be measured and no twinning was observed. The mineral is transparent and has white streak. The mineral does not fluoresce in long- or short-wave ultraviolet light. The Mohs hardness is about 4.5 based on scratch tests. Crystals are brittle with irregular stepped fracture. Cleavage is good on {100} and poor on {001}. The density could not be measured because crystals exceed the density of available

https://doi.org/10.1180/mgm.2024.81 Published online by Cambridge University Press

density fluids. The calculated density is 3.834 g·cm^{-3} for the empirical formula using the single-crystal cell. At room temperature, the mineral is soluble in dilute HCl.

Optically, zincostottite is uniaxial (–) with indices of refraction ω = 1.785(5) and ε = 1.765(5) measured in white light. The mineral is nonpleochroic. The Gladstone-Dale compatibility index (Mandarino, 2007) is 0.051 for the empirical formula in the range of good compatibility.

Raman spectroscopy

Raman spectroscopy was done on a Horiba XploRA PLUS using a 532 nm diode laser, 100 μm slit, 1800 grooves/mm diffraction grating and a 100× (0.9 NA) objective. The spectrum from 4000 to 100 cm^{-1} is compared with that of stottite (RRUFF #R120089) in Figure 2. The spectra are seen to be very similar. The (OH)-stretching bands in the 3400 to 3000 cm^{-1} range are much better resolved in the stottite spectrum. Earlier studies have not attempted to assign specific framework modes to the bands at lower wavenumbers (Kleppe *et al.*, 2012).

Composition

Electron probe microanalyses (EPMA) were done at Caltech on a JXA-iHP200F electron microprobe in WDS mode. The analytical conditions were 15 kV accelerating voltage, 5 nA beam current and 10 μm beam diameter. Analyses fell into two groups, one with almost equal amounts of Zn and Fe and the other with Zn:Fe ≈ 3:1. No zonation of Zn and Fe was observed in the crystals analysed. Below we report the analyses with Zn >> Fe, which are also consistent with the crystal structure refinement reported below. Insufficient material is available for the determination of H_2O, so it is calculated based on the structure (O = 6 and Ge+Si = 1). The crystal structure refinement and OccQP analysis (Wright *et al.*,

https://doi.org/10.1180/mgm.2024.81 Published online by Cambridge University Press

2000) indicate that all Fe in the structure crystal is in the ferric state (and structure refinements on several other zincostottite crystals are also consistent with all Fe being in the ferric state). Consequently, for the EPMA, all Fe has been calculated as +3. Nevertheless, we acknowledge that the presence of some Fe^{2+} is possible in some crystals of zincostottite, but because Fe is not an essential element, its oxidation state is incidental to the definition of the species. There is not enough material for Mössbauer spectroscopy.

The crystals did not take a good polish. The low analytical total is attributed to the somewhat irregular surface. Analytical data are given in Table 2. The empirical formula based on O = 6 atoms per formula unit (*apfu*) is $(Zn_{0.77}Fe^{3+}_{0.23})_{\Sigma 1.00}Ge_{1.00}O_6H_{5.77}$. The ideal formula is $ZnGe(OH)_6$, which requires ZnO 33.91, GeO_2 43.58, H_2O 22.52, total 100 wt%.

X-ray crystallography and structure refinement

X-ray powder diffraction data were recorded using a Rigaku R-Axis Rapid II curved imaging plate microdiffractometer with monochromatized Mo$K\alpha$ radiation. A Gandolfi-like motion on the φ and ω axes was used to randomize the sample. Observed *d*-values and intensities were derived by profile fitting using JADE Pro software (Materials Data, Inc.). The powder data are presented in Table 3. The unit-cell parameters refined from the powder data using JADE Pro with whole-pattern fitting (space group $P4_2/n$) are a = 7.452(3), c = 7.400(4) Å, V = 411.0(4) Å^3.

Single-crystal X-ray studies were done on the same diffractometer and radiation noted above. The Rigaku CrystalClear software package was used for processing the structure data, including the application of an empirical absorption correction using the multi-scan method with ABSCOR (Higashi, 2001). The structure was solved using SHELXT (Sheldrick, 2015a). Neutral atomic scattering factors were used (Wilson, 1992). Refinement proceeded by full-matrix least-squares on F^2 using SHELXL-2016 (Sheldrick, 2015b). The Zn site was refined

https://doi.org/10.1180/mgm.2024.81 Published online by Cambridge University Press

with joint occupancy by Zn and Fe resulting in $Zn_{0.462(13)}Fe_{0.538(13)}$ for a site-scattering value of 111.39±1.45 *e* per unit cell. This compares to a site-scattering value of 116.32*e* per unit cell based on the EPMA ($Zn_{0.77}Fe_{0.23}$). It is worth noting that the structure crystal was checked by EDS following data collection and confirmed to be consistent with the EPMA composition. A possible explanation for the difference is that there is a small vacancy at the site. To test this as well as to confirm the oxidation state of Fe, we analysed the site using OccQP (Wright *et al.*, 2000), a program that uses quadratic equations in a constrained least-squares formulation to optimize occupancy assignments based upon site scattering, chemical composition, charge balance, bond valence and cation-anion bond lengths. With the composition allowed to vary freely among the cations Zn, Fe^{2+} and Fe^{3+}, the optimal site occupancy calculated with OccQP is $Zn_{0.699}Fe^{3+}_{0.265}Fe^{2+}_{0.000}\square_{0.036}$. This occupancy fits the site scattering and cation site valence perfectly. The OccQP occupancy also provides a reasonable fit with the EPMA and confirms all Fe to be +3. The formula based on the OccQP analysis of the Zn site is $(Zn_{0.699}Fe^{3+}_{0.265}\square_{0.036})GeO_6H_{5.807}$. We note that the new Fe^{3+}-dominant stottite-subgroup mineral nancyrossite (Welch *et al.*, 2024a), $Fe^{3+}GeO_6H_5$, was found in the same Ge-rich horizon at Level 30 of the Tsumeb mine from which the zincostottite specimens are presumed to have come.

Difference Fourier synthesis revealed the likely H sites. The H sites were refined with a soft restraint of 0.82(2) Å on the O–H distances and with the U_{eq} set to 1.5 times that of the associated O atoms. The highly directional O-H···O linkages in hydroxyperovskites allow plausible H atoms in the list of difference-Fourier maxima to be recognized (Mitchell *et al.* 2017). Furthermore, it is known that some H sites in hydroxyperovskites are half-occupied (Basciano et al. 1998; Lafuente *et al.* 2015; Welch and Kleppe, 2016; Welch *et al.* 2024b). Hydroxyperovskites with space group $P4_2/n$, such as stottite, have one fully occupied and four half occupied H (Lafuente *et al.*, 2015; Welch and Kleppe, 2016). Zincostottite has one fully

https://doi.org/10.1180/mgm.2024.81 Published online by Cambridge University Press

occupied and four half occupied H sites, as is characteristic of $P4_2/n$ hydroxyperovskites. No evidence of merohedral twinning (0 1 0/1 0 0/0 0 -1) was found in difference-Fourier maps. Also, no superlattice reflections that would indicate ordering of Zn and Fe^{3+} were seen in the diffraction patterns of any of the crystals examined, including those which had nearly equal amounts of Zn and Fe^{3+}.

Data collection and refinement details are given in Table 4, atom coordinates and displacement parameters in Table 5, selected bond distances and angles in Table 6 and a bond valence analysis in Table 7. Note that the Zn-site occupancy indicated by OccQP ($Zn_{0.699}Fe^{3+}_{0.265}\square_{0.036}$) was used for the bond-valence calculations.

Zincostottite is isostructural with stottite (Ross *et al.*, 1988) and other double hydroxyperovskites in the stottite subgroup (Mitchell *et al.*, 2017). The structure is a 3D framework consisting of alternating $Zn(OH)_6$ and $Ge(OH)_6$ octahedra sharing OH corners (Fig. 3). The hydrogen bonding scheme is the same as that delineated by Ross *et al.* (2002) based on O–O bond distances and later confirmed by Kleppe *et al.* (2012) with the determination of H atom positions. Selected data for stottite, zincostottite and nancyrossite are compared in Table 8.

Discussion

Hydroxyperovskites have been recognized as having potential as materials for use in photocatalysis and electrolytic catalysis (Evans et al. 2020). Minerals such as jeanbandyite, $FeSnO_6H_5$, and nancyrossite, $FeGeO_6H_5$, have proton deficiencies (five instead of six H *pfu*) and may have novel H behaviour, such as high proton mobility. Proton conductivity in these materials and related hydroxyperovskites is unexplored. Hydroxyperovskites, in general, are an overlooked group of structures that deserve further attention as potential functional materials.

https://doi.org/10.1180/mgm.2024.81 Published online by Cambridge University Press

Acknowledgements

Two anonymous reviewers and Structures Editor Peter Leverett are thanked for their constructive comments on the manuscript. The EPMA was carried out at the Caltech GPS Division Analytical Facility, which is supported, in part, by NSF Grant EAR-2117942. A portion of this study was funded by the John Jago Trelawney Endowment to the Mineral Sciences Department of the Natural History Museum of Los Angeles County.

References

Basciano, L.C., Peterson, R.C., Roeder, P.L. and Swainson, I. (1998) Description of schoenfliesite, $MgSn(OH)_6$, and roxbyite, $Cu_{1.72}S$, from a 1375 BC shipwreck, and Rietveld neutron-diffraction refeinement of synthetic schoenfliesite, wickmanite, $MnSn(OH)_6$, and burtite $CaSn(OH)_6$. *The Canadian Mineralogist*, **36**, 1203–1210.

Birch, W.D., Pring, A., Reller, A. and Schmalle, H.D. (1993) Bernalite, $Fe(OH)_3$, a new mineral from Broken Hill, New South Wales: Description and structure. *American Mineralogist*, **78**, 827-834.

Evans, H.A. Wu, Y. Seshadri, R. and Cheetham, A.K. (2020) Perovskite-related ReO_3 materials. *Nature Reviews Materials*, **5**, 196–213.

Ferraris G. and Ivaldi G. (1988) Bond valence vs. bond length in O…O hydrogen bonds. *Acta Crystallographica*, **B44**, 341–344.

Gagné, O.C. and Hawthorne, F.C (2015) Comprehensive derivation of bond-valence parameters for ion pairs involving oxygen. *Acta Crystallographica*, **B71**, 562–578.

Gebhard, G. (1999) *Tsumeb II. A Unique Mineral Locality*. GG Publishing, Grossenseifen, Germany.

Higashi, T. (2001) *ABSCOR*. Rigaku Corporation, Tokyo.

https://doi.org/10.1180/mgm.2024.81 Published online by Cambridge University Press

Kleppe, A.K., Welch. M.D., Crichton, W.A. and Jephcoat, A.P. (2012) Phase transitions in hydroxide perovskites: a Raman spectroscopic study of stottite, $FeGe(OH)_6$ to 21 GPa. *Mineralogical Magazine*, **76**, 949–962.

Lafuente, B., Yang, H. & Downs, R.T. (2015) Crystal structure of tetrawickmanite $Mn^{2+}Sn(OH)_6$. *Acta Crystallographica*, **E71**, 234–237.

Mandarino, J.A. (2007) The Gladstone–Dale compatibility of minerals and its use in selecting mineral species for further study. *The Canadian Mineralogist*, **45**, 1307–1324.

Marshukova, N.K., Palovskii, A.B., Sidorenko, G.A. and Christyakova, N.I. (1981) Vismirnovite, $ZnSn(OH)_6$, and natanite, $FeSn(OH)_6$, new tin minerals. *Zapiski Vesesoyuznogo Mineralogicheskogo Obschchestva*, **110**, 492-500.

Mitchell, R.H., Welch, M.D. and Chakmouradian. A.R. (2017) Nomenclature of the perovskite supergroup: A hierarchical system of classification based on crystal structure and composition. *Mineralogical Magazine*, **81**, 411–461.

Morgenstern-Badarau, I. (1976) Effet Jahn-Teller et structure cristalline de l'hydroxide mushistonite $CuSn(OH)_6$. *Journal of Solid State Chemistry*, **17**, 399-406.

Moore, P.B and Smith, J.V. (1967) Wickmanite, $Mn^{+2}[Sn^{+4}(OH)_6]$, a new mineral from Långban. *Arkiv för Mineralogi och Geology*, **4**, 395-399.

Mullica, D.F., Beall, G.W. and Milligan, W.O. (1979) The crystal structure of cubic $In(OH)_3$ by X-ray and neutron diffraction methods. *Journal of Inorganic Nuclear Chemistry* **41**, 277–282.

Ross, C.R., Bernstein, L.R. and Waychunas, G.A. (1988) Crystal-structure refinement of stottite, $FeGe(OH)_6$. *American Mineralogist*, **73**, 657–661.

Ross, N.L., Chaplin, T.D. and Welch, M.D. (2002) Compressibility of stottite, $FeGe(OH)_6$: An octahedral framework with protonated O atoms. *American Mineralogist*, **87**, 1410–1414.

Sheldrick, G.M. (2015a) *SHELXT* - Integrated space-group and crystal-structure determination. *Acta Crystallographica*, **A71**, 3–8.

Sheldrick, G.M. (2015b) Crystal Structure refinement with *SHELX*. *Acta Crystallographica*, **C71**, 3–8.

Von Bezing, L. (2007) *Namibia - Minerals and Localities*. Bode Verlag GmbH, Haltern.

Welch, M.D., Crichton, W.A. and Ross, N.L. (2005) Compression of the perovskite-related mineral bernalite $Fe(OH)_3$ to 9 GPa and a reappraisal of its structure. *Mineralogical Magazine*, **69**, 309-315.

Welch, M.D. and Kleppe, A.K. (2016) Polymorphism of the hydroxide perovskite $Ga(OH)_3$ and possible proton-driven transformational behaviour. *Physics and Chemistry of Minerals*, **43**, 515–526.

Welch, M.D., Najorka, J., Kleppe, A.K., Kampf, A.R. and Spratt. J. (2024a) Nancyrossite, IMA 2024-033. CNMNC Newsletter **81**, *European Journal of Mineralogy*, **36**, in press.

Welch, M.D., Najorka, J. and Wunder, B. (2024b) Crystal structure, hydrogen bonding, and high-pressure behaviour of the hydroxide perovskite $MgSi(OH)_6$: A phase relevant to the deep subduction of hydrated oceanic crust. *American Mineralogist*, **109**, 255–264.

Williams, S.A. (1985) Mopungite, a new mineral from Nevada. *The Mineralogical Record*, **16**, 73-74.

Wilson, A.J.C. (editor) (1992) *International Tables for Crystallography*, *Volume C*. Kluwer Academic Publishers, Dordrecht, The Netherlands.

Wright, S.E., Foley, J.A., and Hughes, J.M. (2000) Optimization of site occupancies in minerals using quadratic programming. *American Mineralogist*, **85**, 524–531.

https://doi.org/10.1180/mgm.2024.81 Published online by Cambridge University Press

Figure 1. Heavily etched zincostottite crystal with chalcocite crystals in vug lined with siderite crystals on cotype specimen (#76278); FOV 1.13 mm across.

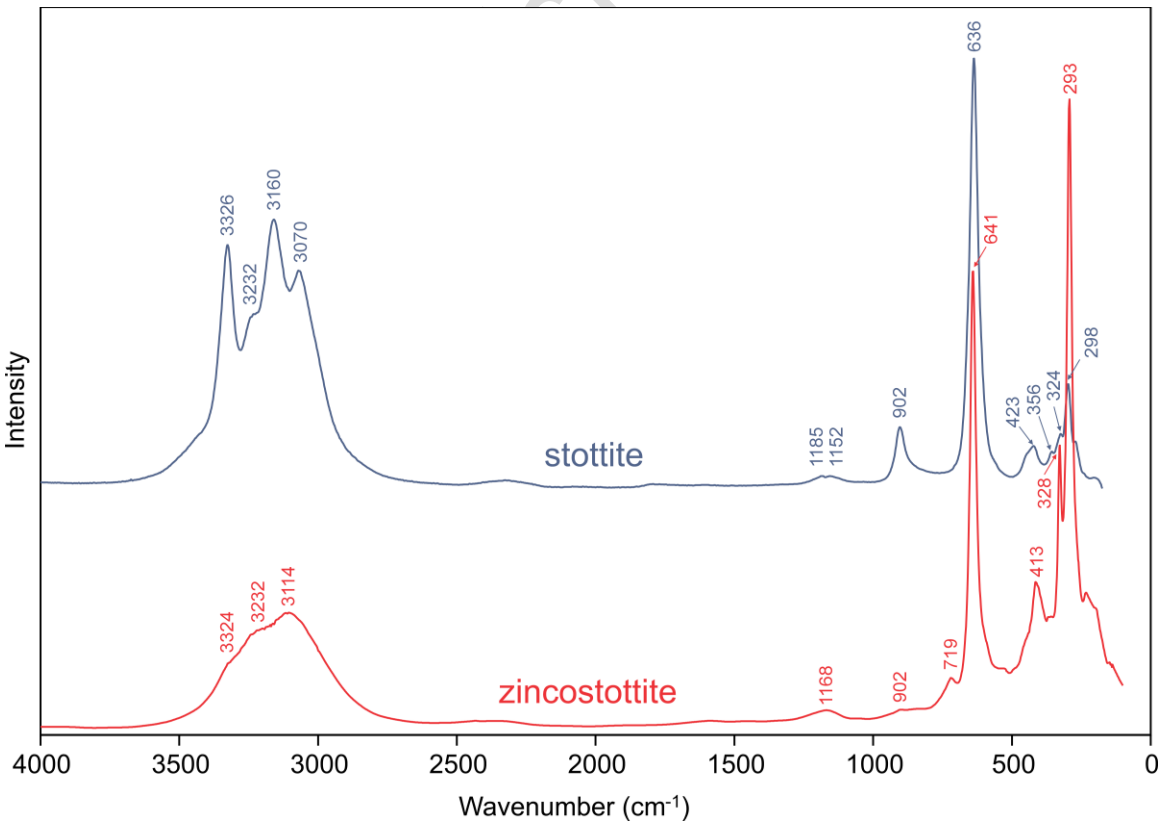

Figure 2. Raman spectra of stottite and zincostottite.

https://doi.org/10.1180/mgm.2024.81 Published online by Cambridge University Press

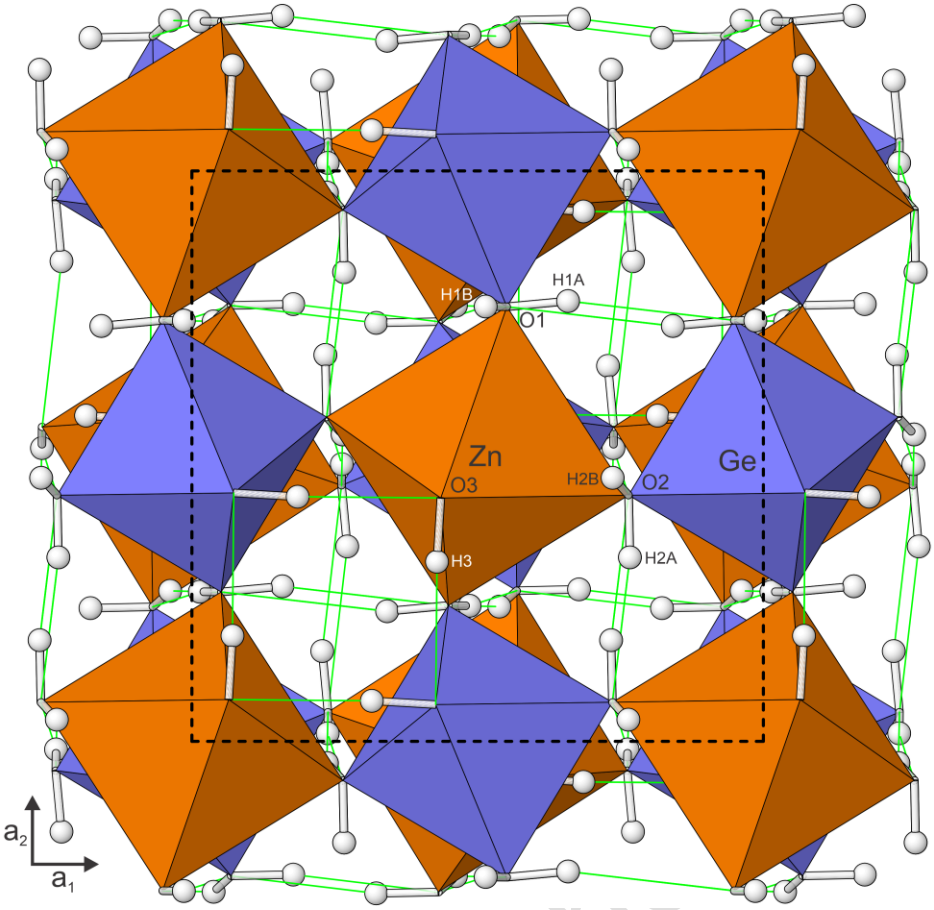

Figure 3. The zincostottite structure viewed down [001]. Hydrogen bonds are shown as light green lines. The unit cell outline is shown with dashed lines.

https://doi.org/10.1180/mgm.2024.81 Published online by Cambridge University Press

Table 1. Natural hydroxyperovskites.

Hydroxyperovskite	Formula	Space group	Reference*
bernalite	$Fe(OH)_3$	*Pmmn*	1,2
söhngeite	$Ga(OH)_3$	$P4_2/nmc$	3
dzahlindite	$In(OH)_3$	*Im*-3	4
schoenfliesite	$MgSn(OH)_6$	*Pn*-3	5
burtite	$CaSn(OH)_6$	*Pn*-3	5
wickmannite	$MnSn(OH)_6$	*Pn*-3	6
tetrawickmannite	$MnSn(OH)_6$	$P4_2/n$	7
natanite	$FeSn(OH)_6$	$P4_2/n$	8
jeanbandyite	$FeSnO(OH)_5$**	$P4_2/n$	9,10
mushistonite	$CuSn(OH)_6$	$P4_2/n$	11,12
vismirnovite	$ZnSn(OH)_6$	*Pn*-3	8
stottite	$FeGe(OH)_6$	$P4_2/n$	13,14
nancyrossite	$FeGeO_6H_5$	$P4_2/n$	15
zincostottite	$ZnGe(OH)_6$	$P4_2/n$	16
mopungite	$NaSb(OH)_6$	$P4_2/n$	17

* Structure
** Formula reported by Welch and Kampf (2017).

[1] Birch *et al.* (1993); [2] Welch *et al.* (2005); [3] Welch & Kleppe (2016); [4] Mullica *et al.* (1979); [5] Basciano *et al.* (1998); [6] Moore & Smith (1967); [7] Lafuente *et al.* (2015); [8] Marshukova *et al.* (1981); [9] Kampf (1982); [10] Welch and Kampf (2017); [11] Morgenstern-Badarau (1976); [12] Najorka *et al.* (2019); [13] Ross *et al.* (1988); [14] Kleppe *et al.* (2012); [15] Welch *et al.* (2024); [16] Kampf *et al.* (2024); [17] Williams (1985).

Table 2. Compositional data in wt% for zincostottite.

Constituent	Mean	Range	S.D.	Probe Standard	Normalized
ZnO	25.14	24.11–25.51	0.46	ZnO	26.42
Fe_2O_3	7.24	7.03–7.60	0.23	fayalite	7.61
GeO_2	41.81	41.61–42.04	0.14	Ge metal	43.95
SiO_2	0.07	0.05–0.08	0.01	fayalite	0.07
H_2O*	20.88				21.95
Total	95.14				100.00

* Based on the structure (O = 6 *apfu*)

https://doi.org/10.1180/mgm.2024.81 Published online by Cambridge University Press

Table 3. Powder X-ray data (*d* in Å) for zincostottite.

I_{obs}	d_{obs}	d_{calc}	I_{calc}	*hkl*
4	4.283	4.292	4	1 1 1
100	3.719	3.726	100	2 0 0
		3.700	46	0 0 2
		3.314	1	1 0 2
2	3.039	3.028	1	1 1 2
45	2.630	2.635	20	2 2 0
		2.626	45	2 0 2
		2.476	1	1 2 2
9	2.350	2.355	6	3 0 1
		2.342	5	1 0 3
5	2.247	2.246	6	3 1 1
15	2.146	2.146	21	2 2 2
		2.062	1	3 0 2
5	1.987	1.991	3	3 2 1
		1.983	3	1 2 3
20	1.860	1.863	18	4 0 0
		1.850	8	0 0 4
		1.804	1	3 2 2
51	1.663	1.664	44	4 0 2
		1.657	22	2 0 4
37	1.518	1.519	30	4 2 2
		1.514	16	2 2 4
		1.434	1	5 1 1
8	1.315	1.317	4	4 4 0
		1.313	6	4 0 4
2	1.274	1.276	1	5 0 3
		1.271	1	3 0 5
		1.259	1	3 5 1
4	1.249	1.241	7	4 4 2
12	1.237	1.238	11	2 4 4
		1.233	1	0 0 6
9	1.176	1.178	8	6 0 2
		1.171	4	2 0 6
11	1.121	1.123	9	2 6 2
		1.117	5	2 2 6
2	1.073	1.073	3	4 4 4
		1.033	2	4 6 0
4	1.031	1.031	2	6 0 4
		1.028	2	4 0 6
		0.995	4	4 6 2
8	0.994	0.994	4	2 6 4
		0.991	4	2 4 6

https://doi.org/10.1180/mgm.2024.81 Published online by Cambridge University Press

Table 4. Data collection and structure refinement details for zincostottite.

Diffractometer	Rigaku R-Axis Rapid II
X-ray radiation	Mo$K\alpha$ (λ = 0.71075 Å)
Temperature	293(2) K
Formula derived from SREF	$(Fe_{0.54}Zn_{0.46})Ge(OH)_6$
Empirical formula (EPMA)	$(Zn_{0.77}Fe^{3+}_{0.23})GeO_6H_{5.78}$
Formula from OccQP	$(Zn_{0.699}Fe^{3+}_{0.265}\square_{0.036})GeO_6H_{5.807}$
Space group	$P4_2/n$ (#86)
Unit cell dimensions	a = 7.4522(18) Å
	c = 7.4000(8) Å
V	411.0(2) Å^3
Z	4
Density (for SREF formula)	3.796 g cm^{-3}
Absorption coefficient	11.84 mm^{-1}
F(000)	455.4
Crystal size	160 × 130 × 50 μm
θ range	3.87 to 30.49°
Index ranges	$-9 \le h \le 9$, $-9 \le k \le 9$, $-9 \le l \le 9$
Refls collected / unique	8553 / 467; R_{int} = 0.050
Reflections with $I > 2\sigma_I$	379
Completeness to θ = 30.49°	99.0%
Refinement method	Full-matrix least-squares on F^2
Parameters / restraints	56 / 5
GoF	1.107
Final R indices [$I > 2\sigma I$]	R_1 = 0.0265, wR_2 = 0.0704
R indices (all data)	R_1 = 0.0399, wR_2 = 0.0772
Largest diff. peak / hole	+0.52 / –0.41 e/A^3

Notes: $R_{int} = \Sigma|F_o^2\text{-}F_o^2(\text{mean})|/\Sigma[F_o^2]$. GoF = $S = \{\Sigma[w(F_o^2-F_c^2)^2]/(n-p)\}^{1/2}$. $R_1 = \Sigma||F_o|\text{-}|F_c||/\Sigma|F_o|$. $wR_2 = \{\Sigma[w(F_o^2-F_c^2)^2]/\Sigma[w(F_o^2)^2]\}^{1/2}$; $w = 1/[\sigma^2(F_o^2) + (aP)^2 + bP]$ where a is 0.032, b is 0.25 and P is $[2F_c^2 + \text{Max}(F_o^2,0)]/3$.

https://doi.org/10.1180/mgm.2024.81 Published online by Cambridge University Press

Table 5. Atom positions, site occupancies and displacement parameters (Å)^2 for zincostottite.

	x/*a*	*y*/*b*	*z*/*c*	U_{eq}/*U_{iso}	Site occupancy
Zn	0	0	0	0.0119(2)	$Zn_{0.462(13)}Fe_{0.538(13)}$
Ge	0.5	0	0	0.00995(16)	1
O1	0.2619(2)	0.4487(3)	0.5801(2)	0.0168(4)	1
H1A	0.272(8)	0.342(3)	0.597(8)	0.025	0.5
H1B	0.262(8)	0.486(7)	0.684(4)	0.025	0.5
O2	0.5685(2)	0.2642(2)	0.5607(2)	0.0160(4)	1
H2A	0.677(3)	0.266(8)	0.575(8)	0.024	0.5
H2B	0.538(8)	0.236(7)	0.664(4)	0.024	0.5
O3	0.4356(2)	0.4267(2)	0.2631(2)	0.0156(4)	1
H3	0.429(4)	0.315(3)	0.251(4)	0.023	1

	U^{11}	U^{22}	U^{33}	U^{23}	U^{13}	U^{12}
Zn	0.0136(3)	0.0107(3)	0.0113(3)	0.00056(14)	-0.00041(15)	-0.00080(16)
Ge	0.0109(2)	0.0093(2)	0.0097(2)	-0.00002(12)	-0.00044(11)	0.00000(13)
Fe	0.0136(3)	0.0107(3)	0.0113(3)	0.00056(14)	-0.00041(15)	-0.00080(16)
O1	0.0133(8)	0.0216(9)	0.0157(9)	0.0023(8)	0.0011(7)	-0.0010(7)
O2	0.0155(9)	0.0140(8)	0.0184(9)	0.0022(7)	0.0000(8)	0.0011(6)
O3	0.0171(9)	0.0128(9)	0.0168(9)	-0.0007(7)	-0.0010(6)	-0.0004(8)

Table 6. Selected bond lengths (Å) for zincostottite.

Zn–O1 (×2)	2.0751(18)	Ge–O2 (×2)	1.8843(17)
Zn–O3 (×2)	2.0781(16)	Ge–O3 (×2)	1.8982(16)
Zn–O2 (×2)	2.0831(17)	Ge–O1 (×2)	1.9096(17)
<Zn–O>	2.0788	<Ge–O>	1.8974

Hydrogen bonds

D–H···*A*	*D*–H	H···*A*	*D*···*A*	<DHA
O1–H1A···O1	0.81(2)	2.18(3)	2.967(4)	163(6)
O1–H1B···O2	0.82(2)	2.00(2)	2.810(3)	174(6)
O2–H2A···O2	0.82(2)	1.91(2)	2.713(4)	166(6)
O2–H2B···O1	0.82(2)	2.01(3)	2.810(3)	165(6)
O3–H3···O3	0.839(19)	1.870(19)	2.708(3)	176(3)

https://doi.org/10.1180/mgm.2024.81 Published online by Cambridge University Press

Table 7. Bond valences analysis for zincostottite. Values are in valence units (*vu*).

	Zn ($Zn_{0.699}Fe^{3+}_{0.265}$)	Ge	Hydrogen bonds		Σ
			donated	accepted	
O1	$0.38^{\times 2\downarrow}$	$0.64^{\times 2\downarrow}$	-0.07, -0.09	0.07, 0.09	1.02
O2	$0.37^{\times 2\downarrow}$	$0.69^{\times 2\downarrow}$	-0.09, -0.11	0.09, 0.11	1.06
O3	$0.38^{\times 2\downarrow}$	$0.66^{\times 2\downarrow}$	-0.22	0.22	1.04
Σ	2.26	3.98			

Bond-valence parameters are from Gagné and Hawthorne (2015). Hydrogen-bond valences are based on O–O bond lengths from Ferraris and Ivaldi (1988). Negative values indicate donated hydrogen-bond valence.

Table 8. Selected data for stottite and zincostottite.

	Stottite	Zincostottite	Nancyrossite
Formula	$Fe^{2+}Ge(OH)_6$	$ZnGe(OH)_6$	$Fe^{3+}GeO_6H_5$
Symmetry	Tetragonal, $P4_2/n$	Tetragonal, $P4_2/n$	Tetragonal, $P4_2/n$
Cell parameters	a = 7.5520(1) Å c = 7.4694(2) Å V = 426.01(6) Å^3	a = 7.4522(18) Å c = 7.4000(8) Å V = 411.0(2) Å^3	a = 7.37382(12) Å c = 7.29704(19) Å V = 396.764(16) Å^3
Z	4	4	4
Fe/Zn–O bond lengths	Fe^{2+}–O1: 2.150(3) Å Fe^{2+}–O2: 2.150(3) Å Fe^{2+}–O3; 2.132(3) Å	Zn–O1: 2.0751(18) Å Zn–O2: 2.0781(16) Å Zn–O3: 2.0831(17) Å	Fe^{3+}–O1: 2.0310(12) Å Fe^{3+}–O2: 2.0265(12) Å Fe^{3+}–O3: 2.0202(10) Å
Reference	Kleppe *et al.*, 2012	This study	2024-033

https://doi.org/10.1180/mgm.2024.81 Published online by Cambridge University Press